Aerospace Science and Technology ••• (••••) •••–•••

Contents lists available at ScienceDirect

Aerospace Science and Technology

www.elsevier.com/locate/aescte

# RANS analysis of the low-Reynolds number flow around the SD7003 airfoil

P. Catalano [a,*,1], R. Tognaccini [b,2]

[a] CIRA, Italian Aerospace Research Center, Via Maiorise, Capua (CE), 81043, Italy
[b] University "Federico II", Naples 80125, Italy

ARTICLE INFO

*Article history:*
Received 29 July 2010
Received in revised form 2 December 2010
Accepted 19 December 2010
Available online xxxx

*Keywords:*
Low-Reynolds
Transition location
RANS

ABSTRACT

This paper presents a numerical analysis of the incompressible flow at Reynolds number $6.0 \times 10^4$ around the Selig–Donovan 7003 airfoil. The airfoil performances have been computed by the Reynolds averaged Navier–Stokes equations and large eddy simulations. The airfoil stall and preliminary post-stall have been obtained by both the methods. Some limitations of the RANS turbulence models for low-Reynolds number flows have been overcome by the $\kappa$–$\omega$ SST-LR model, a recent modification of the well-known SST model. Large-eddy simulations have also been performed for a more detailed analysis of the results. The relevance in the stall mechanism of the laminar separation bubble arising on the airfoil is highlighted. The stall occurs when the laminar bubble present in the leading edge zone and a separated region forming on the central part of the airfoil join together. The $\kappa$–$\omega$ SST-LR model returns the same stall mechanism as the large eddy simulation. Flows at low-Reynolds numbers can be simulated by the RANS methods, but the choice of the turbulence model is crucial. The $\kappa$–$\omega$ SST-LR model has provided results in good agreement with the large eddy simulation and the available experimental data.




## 1. Introduction

This paper presents a numerical investigation of the incompressible flow at Reynolds number $6.0 \times 10^4$ around the Selig–Donovan (SD) 7003 airfoil. The SD 7003 airfoil exhibits a laminar separation bubble (LSB) over a wide range of incidences, and has been the subject of numerical and experimental [18,1] campaigns. In this paper the focus is placed on the evolution of the LSB, on the stall mechanism of the airfoil, and on the possibility to predict these phenomena by a Reynolds averaged Navier–Stokes (RANS) method.

Flows at Reynolds number $10^4$–$10^5$ are encountered in many applications, i.e. unmanned and micro-aerial vehicles. The numerical simulations of these kind of flows are still challenging. The presence of laminar separation bubbles is hard to be detected. Few efforts have been spent to calibrate RANS turbulence models for flows at low-Reynolds number. Finally the presence of large laminar regions makes the prediction of the transition zone particularly crucial.

Most of the simulations found in literature have been intended to investigate the capability of a numerical method to reproduce a laminar separation bubble. Windte [27], Radespiel [19], Yuan et al. [28] employed a RANS solver coupled to a transition prediction method. These results were achieved by the Menter BSL-two layer model [17], the explicit algebraic Reynolds stress model by Wallin [24], and the Wilcox RSM model [26]. Tang [23] computed the flow at $\alpha = 4°$ by the RANS equations without any particular treatment of the transition. The results are dependent on the turbulence model. Good results are achieved by the Spalart–Allmars model. A too short bubble is instead returned by the Menter BSL-two layer, and the Jones–Launder [12] $\kappa$–$\varepsilon$ models.

Large-eddy simulations of the flow around the SD 7003 airfoil have also been performed. Yuan et al. [28] employed an incompressible solver using the SIMPLE algorithm [8] for the pressure-velocity coupling. The static Smagorinsky and the selective scale model by Lenormand et al. [14] have been used as sub-grid closures of the Navier–Stokes equations. The flow at $Re = 6 \times 10^4$, and $\alpha = 4°$ has been computed. Differences with respect to RANS results in the zone of the bubble in terms of pressure and friction coefficients are shown.

Galbraith and Visbal [9] applied a high-order implicit LES and computed the flow around the SD 7003 airfoil at several incidences. A good comparison with the experimental data is shown. The stall of the SD 7003 airfoil has also been computed.

Catalano and Tognaccini [3] performed RANS and large eddy simulations of the flow at $Re = 6 \times 10^4$ around the SD 7003 air-

* Corresponding author.
*E-mail addresses:* p.catalano@cira.it (P. Catalano), rtogna@unina.it (R. Tognaccini).
*URLs:* http://www.cira.it (P. Catalano), http://www.unina.it (R. Tognaccini).
[1] Research Engineer, PhD, Department of Physics of Fluids.
[2] Associate Professor, Dipartimento di Ingegneria Aerospaziale.

1270-9638/$ – see front matter 
doi:10.1016/j.ast.2010.12.006

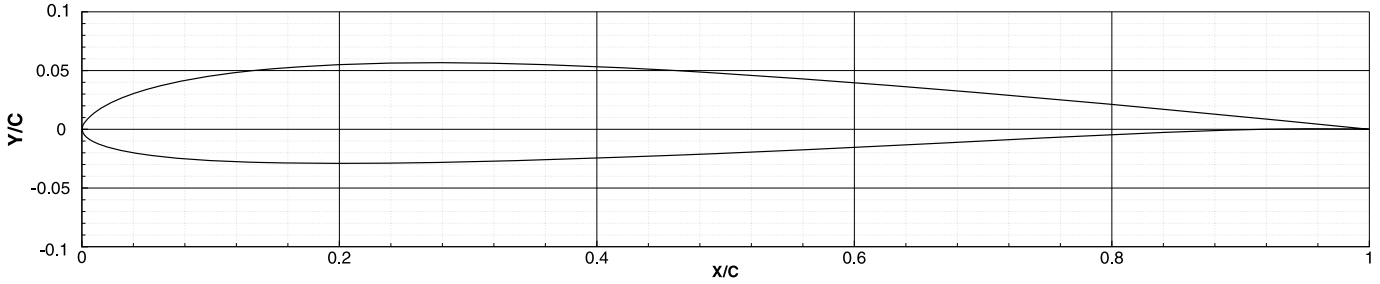


**Fig. 1.** Geometry of the SD7003 airfoil.

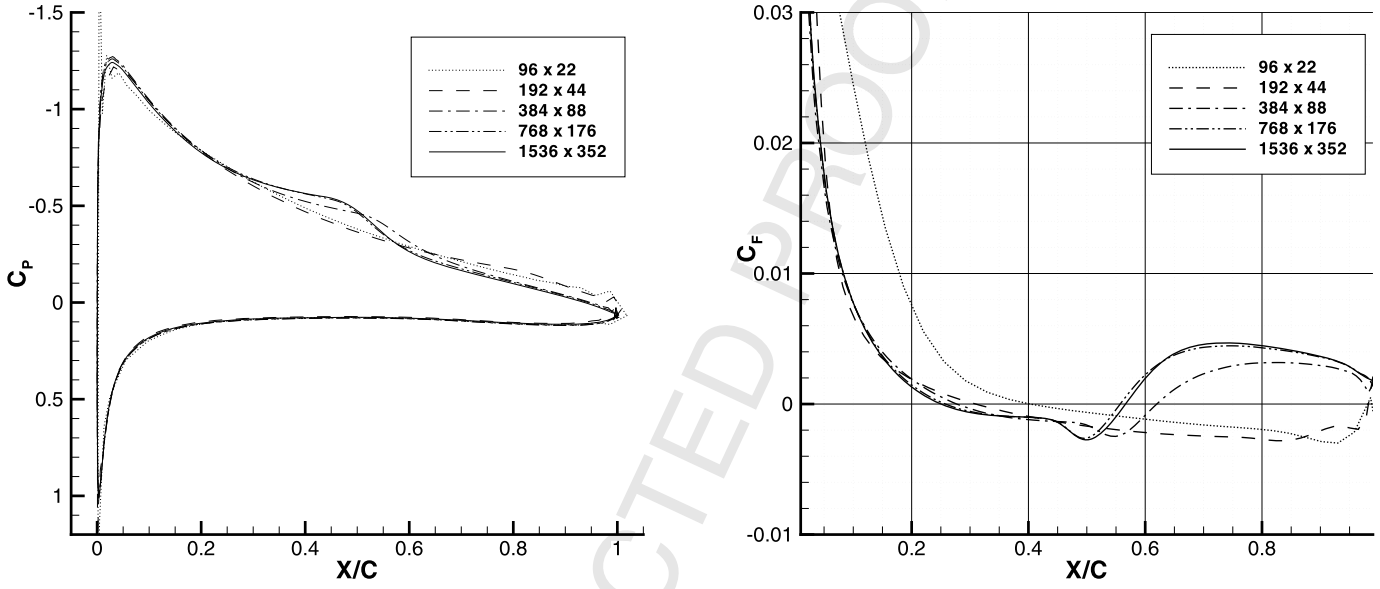


(a) Pressure Coefficient (b) Friction Coefficient

**Fig. 2.** SD7003 airfoil, $Re = 6 \times 10^4$, $\alpha = 4°$. Grid convergence study for the $\kappa$–$\omega$ SST-LR turbulence model. ·····: 96 × 22 cells, – – – –: 192 × 44 cells, –·–·–: 384 × 88 cells, –··–··–: 768 × 176 cells, —: 1536 × 352 cells.



foil at low and moderate incidences. They have shown that the laminar separation bubbles can be detected by a RANS method without any particular treatment of the laminar-turbulent transition. However, very low values of the free-stream turbulence have to be used. Some limitations of the adopted turbulence models have been evidenced as also pointed out by Rumsey and Spalart [20]. In particular, it was observed that the standard $\kappa$–$\omega$ SST model provides a poor result in case of the flow around the SD 7003 airfoil at Reynolds number $6.0 \times 10^4$ and $\alpha = 4°$ if the transition location is specified inside the bubble by a separate method.

Catalano and Tognaccini in a recent paper [5] have proposed a modification of the $\kappa$–$\omega$ SST turbulence model aimed at improving the performances of the model for low-Reynolds number flows. This modified model, re-called here as $\kappa$–$\omega$ SST-LR, is able to correctly reproduce the wall-law velocity for attached flows also in case of low-Reynolds numbers. This model well reproduced at moderate incidences the LSB on the SD7003 airfoil at $Re_\infty = 6.0 \times 10^4$ with a very good agreement with LES data in case of specified transition.

In the present paper, the $\kappa$–$\omega$ SST-LR, is applied to compute the lift and drag curves of the SD 7003 airfoil at Reynolds number $6.0 \times 10^4$ at high angles of attack. The mechanism of the stall is also discussed by comparing RANS results with large-eddy simulations data found in literature [9] and performed by the authors.

The final RANS calculations have been obtained without any *a priori* knowledge of the transition location by an *engineering* criterion, here proposed.

## 2. Numerical methods

### 2.1. Unsteady Reynolds averaged Navier–Stokes solver

A multi-block, efficient and well assessed computational tool for the analysis of complex configurations in the subsonic, transonic, and supersonic regimes [2] is used for the RANS and URANS computations. The equations are discretized by means of a standard cell-centered finite volume scheme with blended self-adaptive second and fourth order artificial dissipation. The time integration is based on the dual-time stepping method (DTS) where a pseudo steady-state problem is solved at each physical time step [16]. The pseudo-time marching advancement is performed by using the Runge–Kutta algorithm with convergence accelerators such as the multi-grid and residual smoothing techniques.

The turbulence equations are weakly coupled with the RANS equations and only solved on the finest grid level of a multi-grid cycle. The standard $\kappa$–$\omega$ SST [17], and SST-LR [5] turbulence models are applied for the simulations discussed in this paper.

Please cite this article in press as: P. Catalano, R. Tognaccini, RANS analysis of the low-Reynolds number flow around the SD7003 airfoil, Aerospace Science and Technology (2011), doi:10.1016/j.ast.2010.12.006

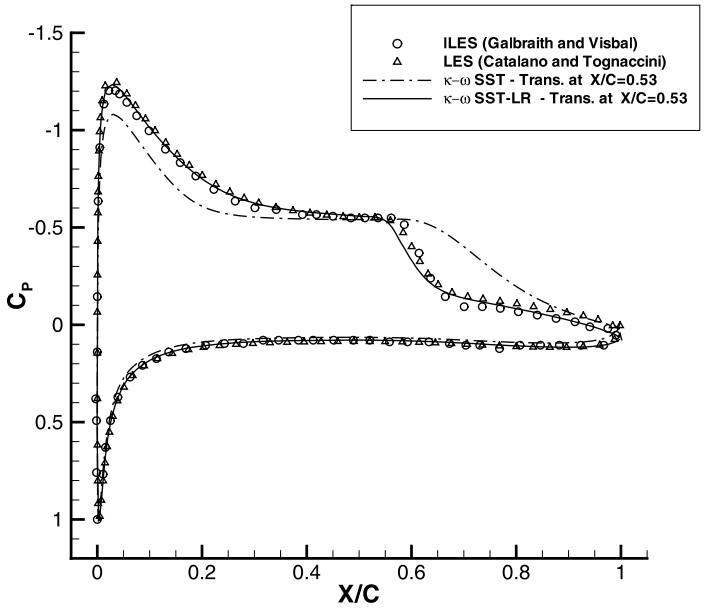


(a) Pressure Coefficient

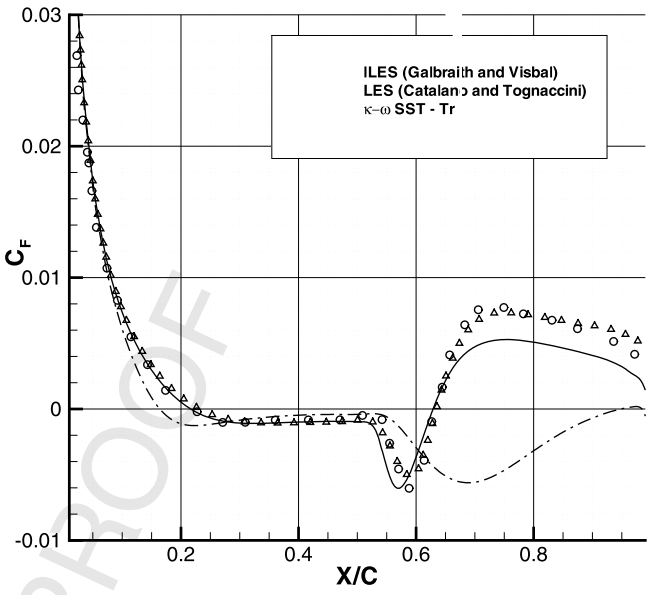




Please cite this article in press as: P. Catalano, R. Tognaccini, RANS analysis of the low-Reynolds number flow around the SD7003 airfoil, Aerospace Science and Technology (2011), doi:10.1016/j.ast.2010.12.006

### 2.2. Large eddy simulation solver

An incompressible flow solver of the Navier–Stokes equations is used for the large eddy simulations [25,6]. The code employs an energy-conservative numerical scheme. Second order central differences in stream-wise and wall-normal directions, and Fourier collocations in the span-wise direction are used. The code is written in body-fitted coordinates with a staggered arrangement of the flow variables. The fractional step approach [13], in combination with the Crank–Nicholson method for the viscous terms and the 3rd order Runge–Kutta scheme is used for the time advancement. The continuity constraint is imposed at each Runge–Kutta substep by solving a Poisson equation for the pressure. The sub-grid scale stress tensor is modeled by the dynamic Smagorinsky model [10] in combination with a least-contraction and span-wise averaging [15].

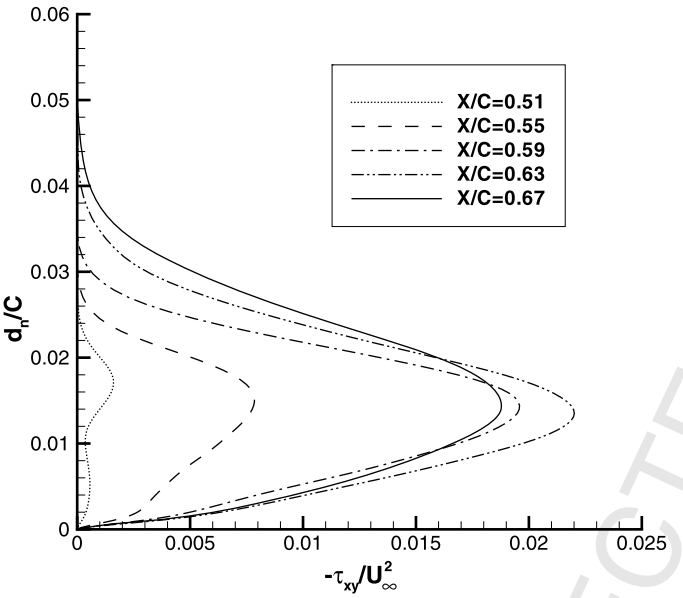


**Fig. 5.** SD 7003 airfoil at Reynolds number $6.0 \times 10^4$ and $\alpha = 4°$: Reynolds shear stress by LES performed by the authors.

## 3. Results and discussion

The incompressible flow around the SD 7003 airfoil (Fig. 1) is computed by RANS and LES techniques. A C-topology grid with

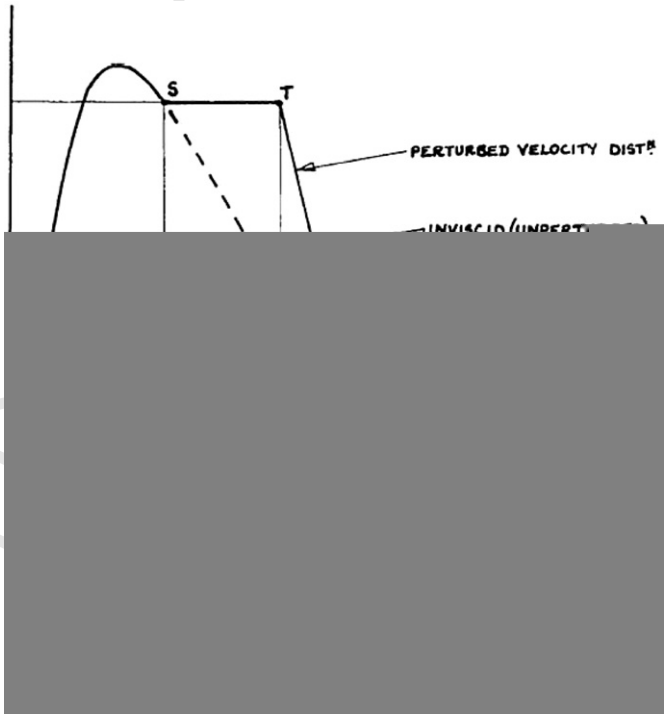


**Fig. 7.** Simplified model of a laminar separation bubble (from p. 29 of [11]).

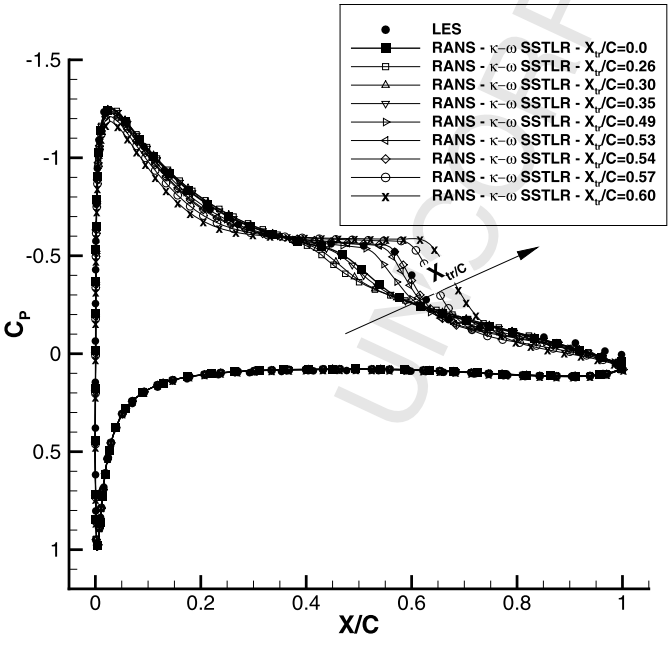


(a) Pressure Coefficient

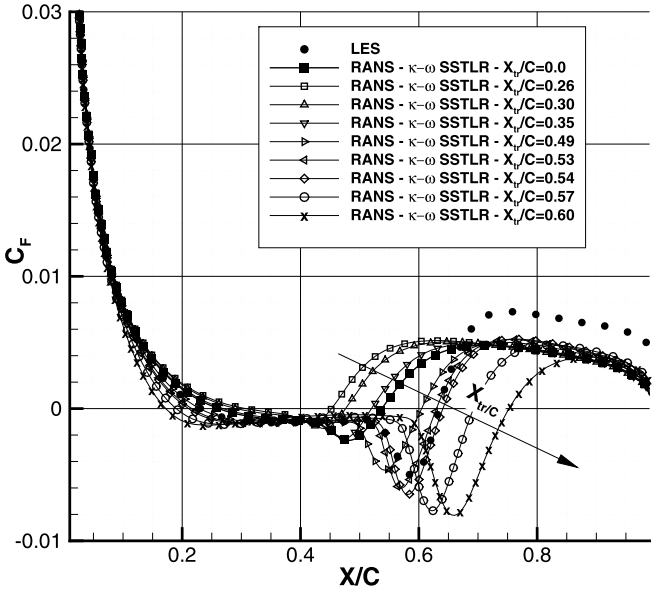


(b) Friction Coefficient

**Fig. 6.** SD7003 airfoil, $Re = 6.0 \times 10^4$, $\alpha = 4°$: effect of the transition location; ●: large-eddy simulation, ■: RANS $X_{tr}/C = 0.0$, □: RANS $X_{tr}/C = 0.26$, △: RANS $X_{tr}/C = 0.30$, ▽: RANS $X_{tr}/C = 0.35$, ▷: RANS $X_{tr}/C = 0.49$, ◁: RANS $X_{tr}/C = 0.53$, ◇: RANS $X_{tr}/C = 0.54$, ○: RANS $X_{tr}/C = 0.57$, ×: RANS $X_{tr}/C = 0.60$.



Please cite this article in press as: P. Catalano, R. Tognaccini, RANS analysis of the low-Reynolds number flow around the SD7003 airfoil, Aerospace Science and Technology (2011), doi:10.1016/j.ast.2010.12.006

768 (96 in the wake) cells in the stream-wise and 176 cells in the normal-to-the-wall direction is used for RANS computations.

A grid convergence study of the RANS simulations has been performed (Fig. 2). The $\kappa$–$\omega$ SST-LR turbulence model has been applied to the flow at $\alpha = 4°$ with the transition location not specified. The turbulent intensity is set $10^{-4}$% and the ratio between the free-stream turbulent and molecular viscosity to $10^{-9}$. The number of point of the computational grid has been doubled starting from a mesh of $96 \times 22$ cells up to a grid with $1536 \times 352$ cells. It has been verified that the pressure and friction coefficients achieved by using the $768 \times 176$ and $1536 \times 352$ grids are almost identical. A negligible difference is present only in the friction coefficients at the re-attachment point. Therefore, a mesh with $768 \times 176$ cells has been considered sufficiently accurate and used for the simulations discussed hereafter.

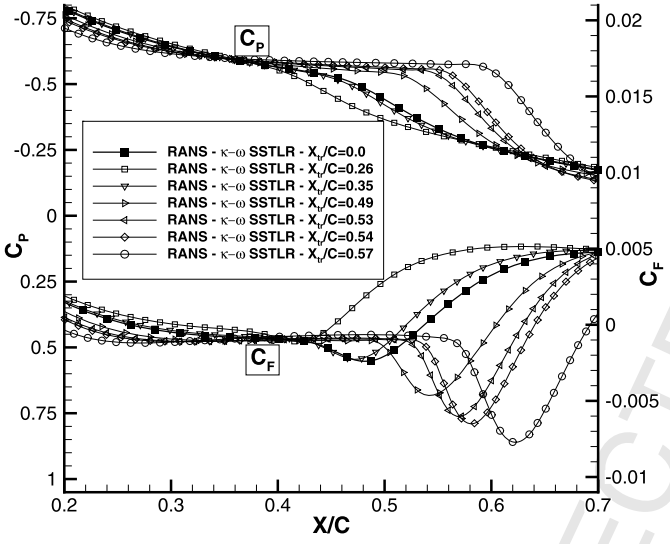


**Fig. 8.** SD7003 airfoil, $Re = 6.0 \times 10^4$, $\alpha = 4°$: pressure and friction coefficient in the zone of the laminar separation bubble; ■: RANS $X_{tr}/C = 0.0$, □: RANS $X_{tr}/C = 0.26$, ▽: RANS $X_{tr}/C = 0.35$, ▷: RANS $X_{tr}/C = 0.49$, ◁: RANS $X_{tr}/C = 0.53$, ◇: RANS $X_{tr}/C = 0.54$, ○: RANS $X_{tr}/C = 0.57$.

For the large-eddy simulation at $\alpha \leqslant 9°$, the computational domain has a span-wise extension $L_z = 0.1 \times C$ ($C$ is the chord of the airfoil) with 864 cells in the stream-wise, 208 in the cross-wise, and 48 in the span-wise $z$ direction. The wall-adjacent cells in wall-units coordinate have size less than one in the wall-normal direction, and order of magnitude 10 in the stream and span-wise directions.

### 3.1. Laminar separation bubble

The $\kappa$–$\omega$ SST, and SST-LR models have been applied to compute the flow around the SD 7003 airfoil at Reynolds number $6 \times 10^4$ and several angles of attack. The results obtained by $\kappa$–$\omega$ SST and SST-LR at $\alpha = 4°$ are compared with the implicit LES by Galbraith and Visbal [9] and the explicit large-eddy simulations performed by the authors [3] in Fig. 3. The transition is fixed at $X_{tr}/C = 0.53$ according to the experimental [18] and numerical [28,9] data found in literature. Only the $\kappa$–$\omega$ SST-LR is in good agreement with the large-eddy simulations.

The Reynolds shear stress and the size of the laminar separation bubble achieved by the $\kappa$–$\omega$ SST-LR qualitatively well compare to the experimental data obtained by the Technical University at Braunschweig [18] as shown in Fig. 4. In this experiment, the transition of the flow has been measured at $X_{tr}/C = 0.53$ and the free-stream turbulence is 0.1%. The numerical and experimental fields are quite similar, and the same order of magnitude of the shear stress is observed. In the numerical simulation, the flow separates at $X/C = 0.21$, while the measured separation point is $X/C = 0.30$. The re-attachment point is in better agreement; $X/C = 0.64$ in the simulation and $X/C = 0.62$ in the experiment. The height of the bubble seems to be slightly over-predicted.

### 3.2. Transition location

Several data are available in literature for the transition location of the flow at $Re = 6 \times 10^4$ and $\alpha = 4°$ around the SD 7003 airfoil.

Experiments [18] have been performed at the Low-Reynolds Number Tow Tank of the Institute for Aerospace Research (IAR), at the Low-Noise Wind Tunnel of the Technical University of Braunschweig (TU-BS), and at the Horizontal Free-Surface Water Tunnel

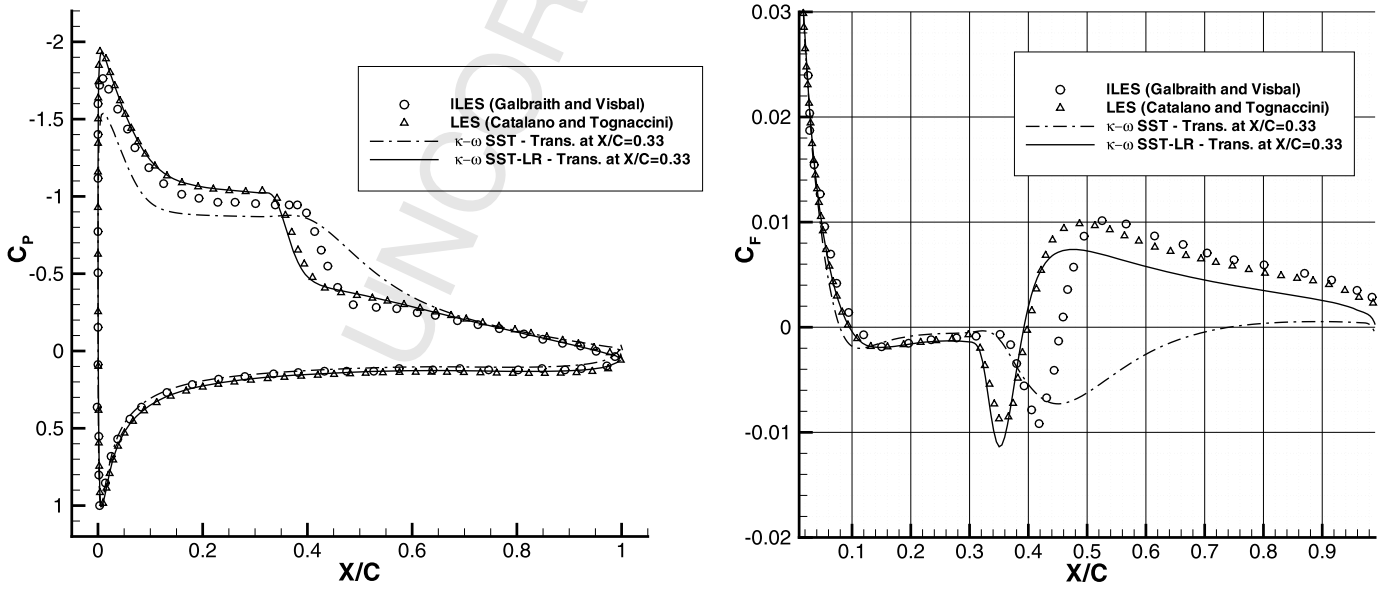


(a) Pressure Coefficient (b) Friction Coefficient

**Fig. 9.** SD7003 airfoil, $Re = 6 \times 10^4$, $\alpha = 6°$. Pressure and friction coefficient; ○: ILES (Galbraith and Visbal), △: LES (Catalano and Tognaccini), – · – ·: RANS $\kappa$–$\omega$ SST transition point fixed ($X_{tr}/C = 0.33$), —: RANS $\kappa$–$\omega$ SST-LR transition point fixed ($X_{tr}/C = 0.33$).



Please cite this article in press as: P. Catalano, R. Tognaccini, RANS analysis of the low-Reynolds number flow around the SD7003 airfoil, Aerospace Science and Technology (2011), doi:10.1016/j.ast.2010.12.006

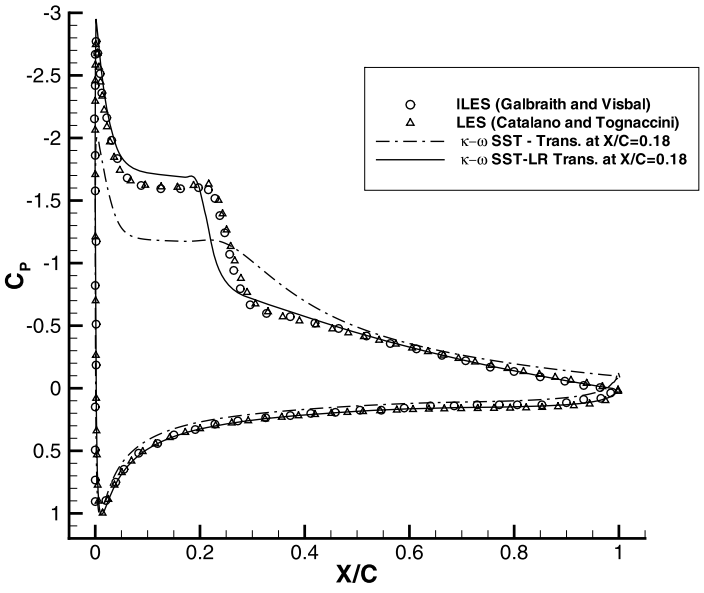


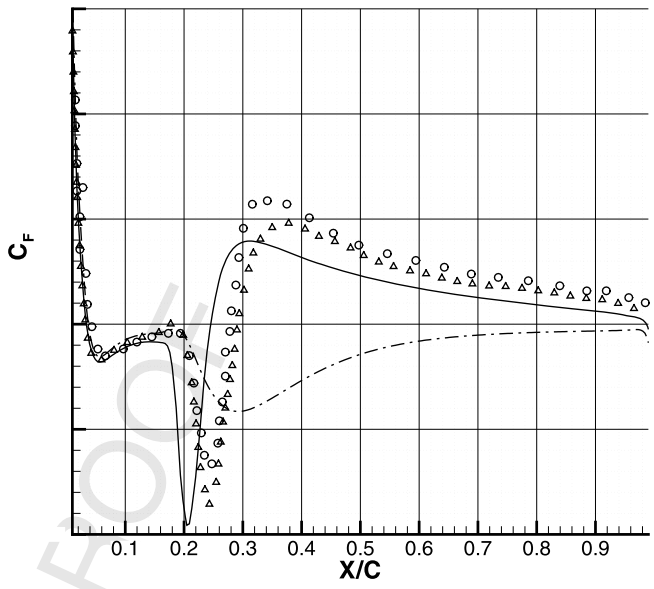


(a) Pressure Coefficient



Please cite this article in press as: P. Catalano, R. Tognaccini, RANS analysis of the low-Reynolds number flow around the SD7003 airfoil, Aerospace Science and Technology (2011), doi:10.1016/j.ast.2010.12.006

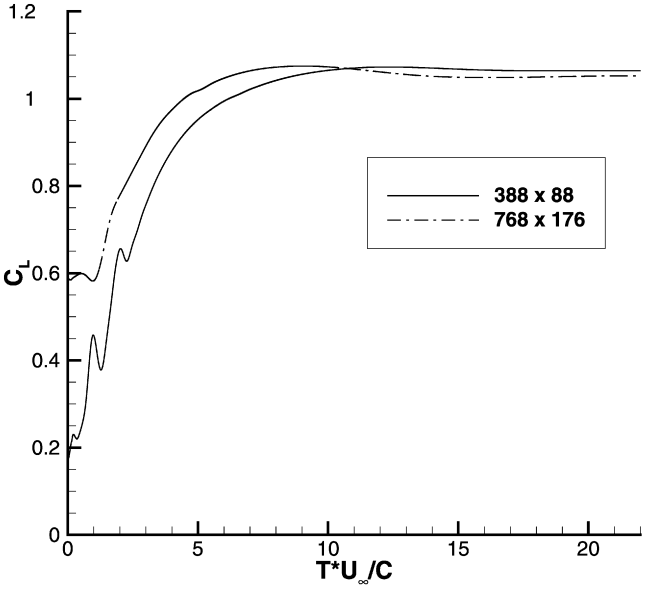


(a) Lift Coefficient

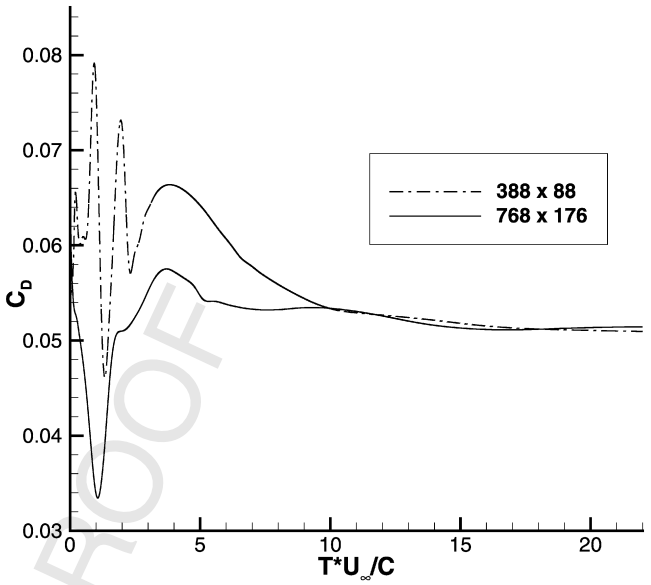


(b) Drag Coefficient

**Fig. 14.** SD 7003 airfoil at Reynolds number $6.0 \times 10^4$ and $\alpha = 10°$: URANS — $\kappa$–$\omega$ SST-LR turbulence model; —: 388 × 88 cells, – · – · –: 768 × 176 cells.

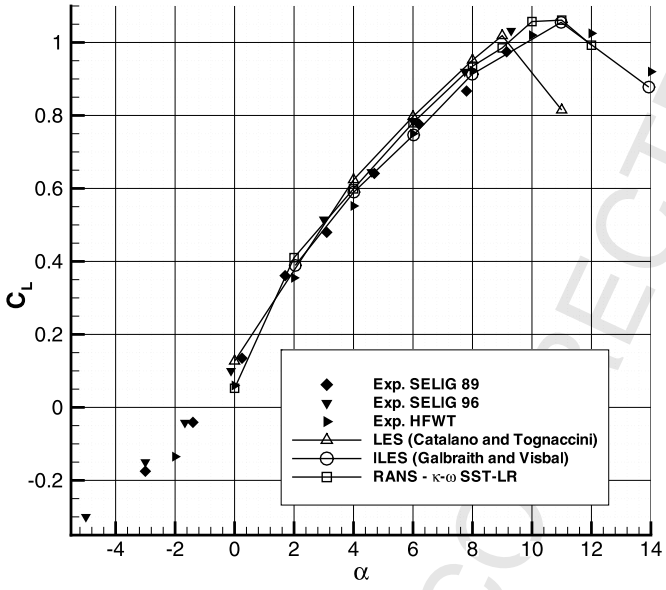


**Fig. 15.** SD7003 airfoil: lift curve at $Re = 6.0 \times 10^4$; full symbols: experiments, —○—: implicit large-eddy simulation (Galbraith and Visbal), —◇—: large-eddy simulation (Catalano and Tognaccini), —□—: RANS $\kappa$–$\omega$ SST-LR.

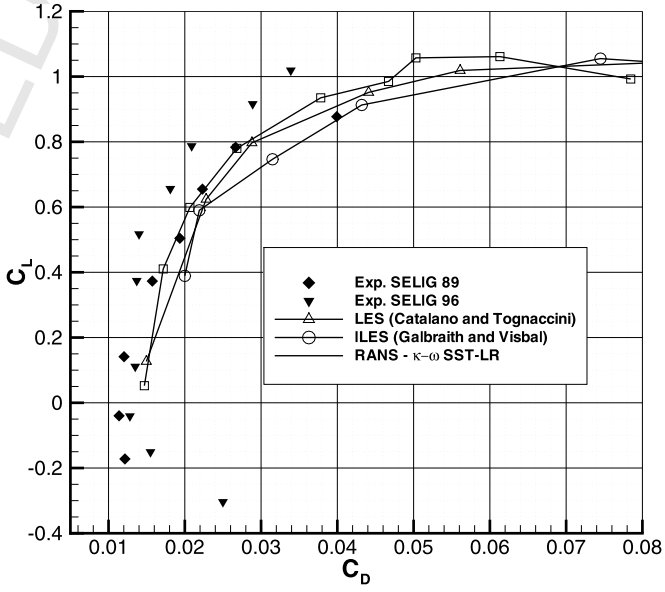


**Fig. 16.** SD7003 airfoil: drag polar at $Re = 6.0 \times 10^4$; full symbols: experiments, —○—: implicit large-eddy simulation (Galbraith and Visbal), —△—: large-eddy simulation (Catalano and Tognaccini), —□—: RANS $\kappa$–$\omega$ SST-LR.

friction coefficients achieved by the $\kappa$–$\omega$ SST-LR are in very good agreement with the LES data by the authors, but again this is not the case by the standard SST model. The transition has been imposed at $X_{tr}/C = 0.33$ for $\alpha = 6°$, $X_{tr}/C = 0.18$ for $\alpha = 8°$, and $X_{tr}/C = 0.13$ for $\alpha = 9°$. These points are in reasonable agreement with Radespiel et al. [19] that obtained a transition location between 0.14 and 0.17 for the flow at $\alpha = 8°$, and with Galbraith and Visbal [9] that report $X_{tr}/C = 0.34$ and $X_{tr}/C = 0.18$ for $\alpha = 6°$ and 8° respectively.

The large-eddy simulations by the authors provide a shear stress field indicating a transition occurring in the same range (Fig. 12). At $\alpha = 6°$, a rapid increase of the $\tau_{xy}$ is visible between the 26% and 30% of the chord, while at $\alpha = 8°$ the shear stress is not negligible at $X/C = 0.18$ and has almost reached the maximum at $X/C = 0.22$.

The Reynolds shear stresses computed by the $\kappa$–$\omega$ SST-LR model are also presented in Fig. 12. At $\alpha = 6°$, a very good agreement with LES data is obtained at all the locations except at $X/C = 0.26$ and $X/C = 0.30$ where the Reynolds shear stress provided by the RANS simulation is negligible. At $\alpha = 8°$, the RANS shear-stress has the maximum slightly upstream with respect to the LES data. This is due to the fact that the bubble provided by the $\kappa$–$\omega$ SST-LR is shorter than the one achieved in the large-eddy simulation (see Fig. 10). However, both RANS and LES data present stresses that increase to a maximum inside the separated region, and start to decrease as soon as the flow reattaches.

The transition locations evaluated by the presented criterion compare well to the results found in literature and obtained by the free software Xfoil [7] (Fig. 13). The authors have not been able to obtain reliable results at high incidences by Xfoil.



Please cite this article in press as: P. Catalano, R. Tognaccini, RANS analysis of the low-Reynolds number flow around the SD7003 airfoil, Aerospace Science and Technology (2011), doi:10.1016/j.ast.2010.12.006

### 3.3. Aerodynamic coefficients

The drag and lift curves of the SD 7003 airfoil at Reynolds number $6.0 \times 10^4$ have been computed by the $\kappa$–$\omega$ SST-LR model [4]. RANS simulations up to $\alpha = 9°$, and time-accurate URANS simulations from $\alpha = 10°$ to 12° have been carried out. Even in case of URANS simulations, steady state solutions are obtained. Fig. 14 shows the evolution in time of the lift and drag coefficient at $\alpha = 10°$. The difference between the grids with $388 \times 88$ and $768 \times 176$ cells is 0.7% for the $C_L$ and less than 2% ($\approx 10$ drag counts) for the $C_D$. These differences do not affect significantly the considerations reported in the following sections. Therefore the URANS simulations have been performed on the mesh with $388 \times 88$ cells to save CPU time.

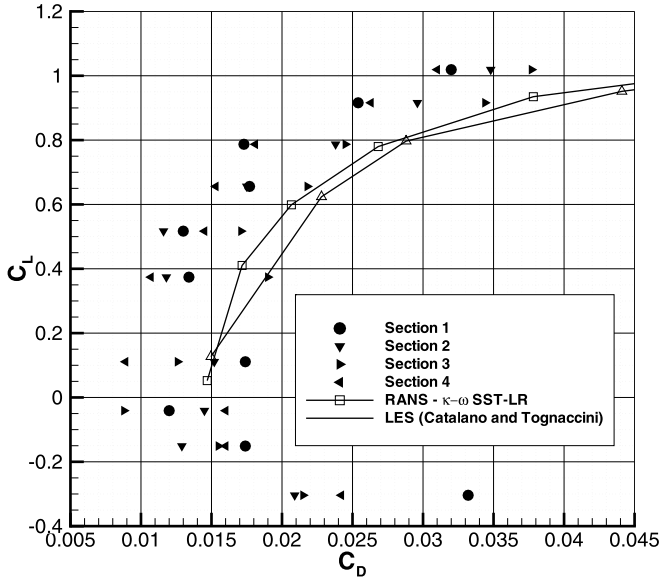


**Fig. 17.** SD7003 airfoil: drag polar at $Re = 6.0 \times 10^4$ by Selig et al. [22]; full symbols: measurements at four different section of the model, –△–: large-eddy simulation (Catalano and Tognaccini), –□–: RANS $\kappa$–$\omega$ SST-LR.

Large-eddy simulations have also been performed up to $\alpha = 11°$. The span-wise extension $L_z$ of the computational domain is $0.1 \times C$ for $\alpha \leqslant 9°$ and $0.2 \times C$ for $\alpha > 9°$. The number of cells used in the span-wise direction is 48 for $L_z = 0.1$, and 96 for $L_z = 0.2$. The simulations are started from a RANS flow field. The solution is preliminary advanced in time with a specified Courant number and a time step computed on the basis of numerical stability analysis. Subsequently, a constant time step $\Delta t = 0.5 \times 10^{-4}$ is used.

#### 3.3.1. Lift coefficient

The lift coefficient is compared to three sets of experimental data, and to the numerical results obtained by the ILES approach [9] in Fig. 15. The measurements taken from Selig et al. [21] at University of Princeton in 1989, from Selig et al. [22] at University of Illinois in 1996, and from Ol et al. [18] at the Horizontal Fee-Surface Wind Tunnel (HFWT) of the Air Force Research Laboratory in 2005 are considered.

At low-medium incidences, the computed lift coefficients compare well with the experimental data. Our large-eddy simulations slightly over-predict the ILES (maximum variation is 6% at $\alpha = 6°$) and experimental results (maximum variation is 10% with respect

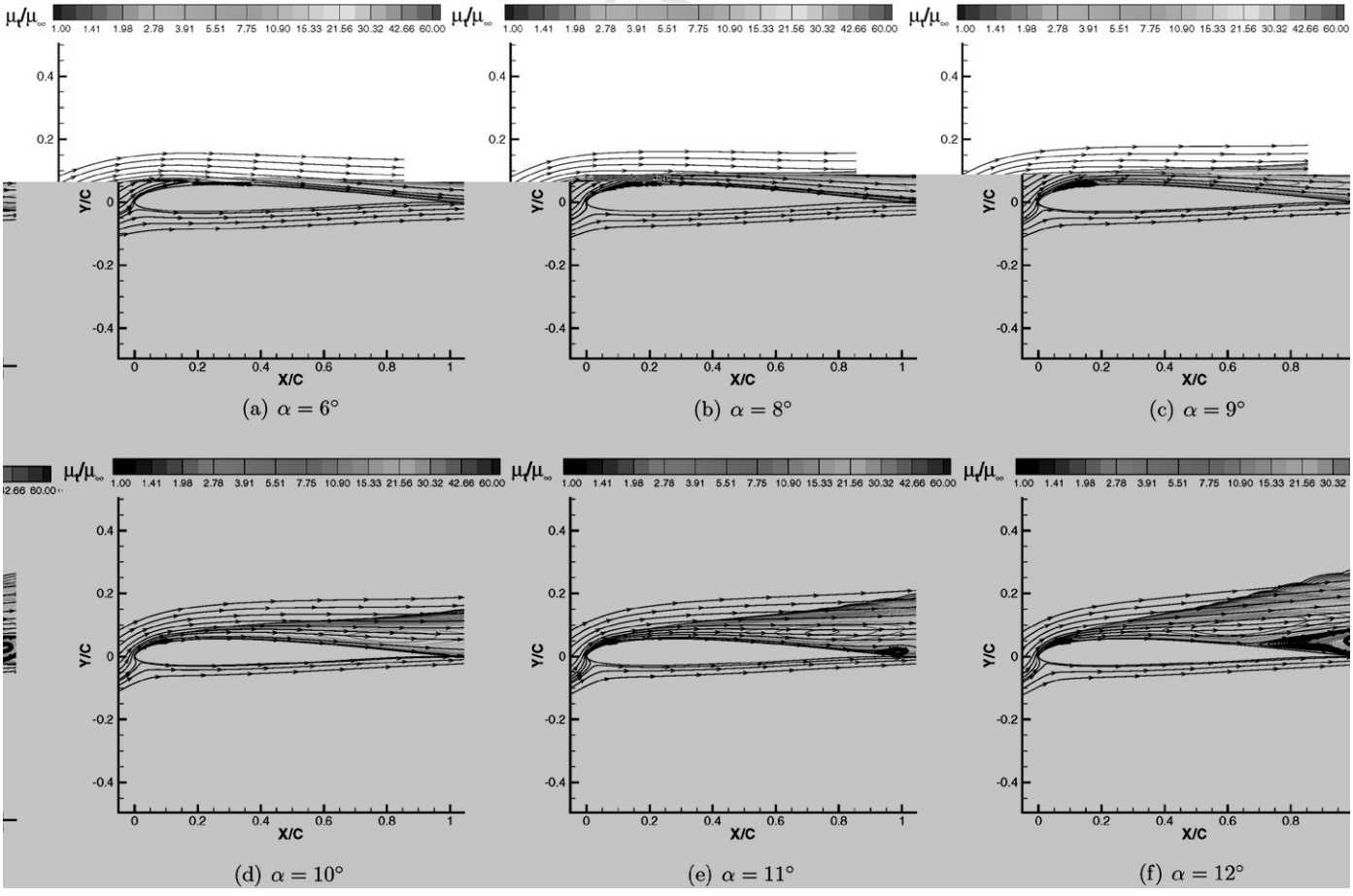


**Fig. 18.** SD7003 airfoil, $Re = 6 \times 10^4$. Streamlines and contour map of the eddy viscosity.

Please cite this article in press as: P. Catalano, R. Tognaccini, RANS analysis of the low-Reynolds number flow around the SD7003 airfoil, Aerospace Science and Technology (2011), doi:10.1016/j.ast.2010.12.006

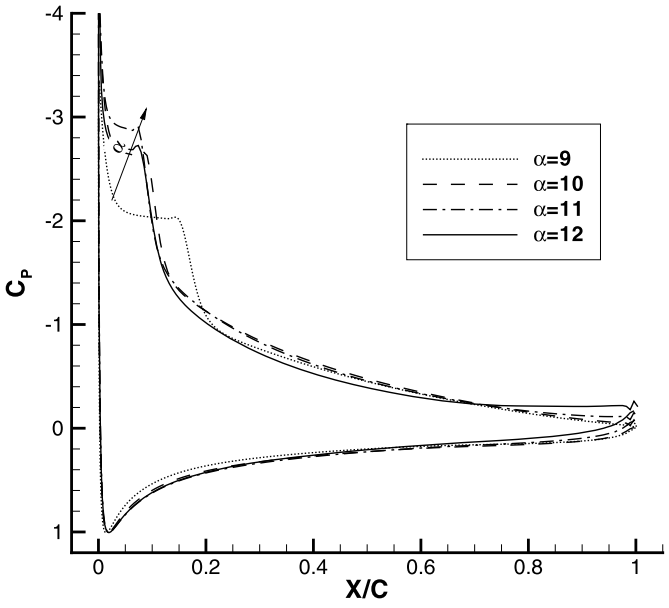


(a) Pressure Coefficient

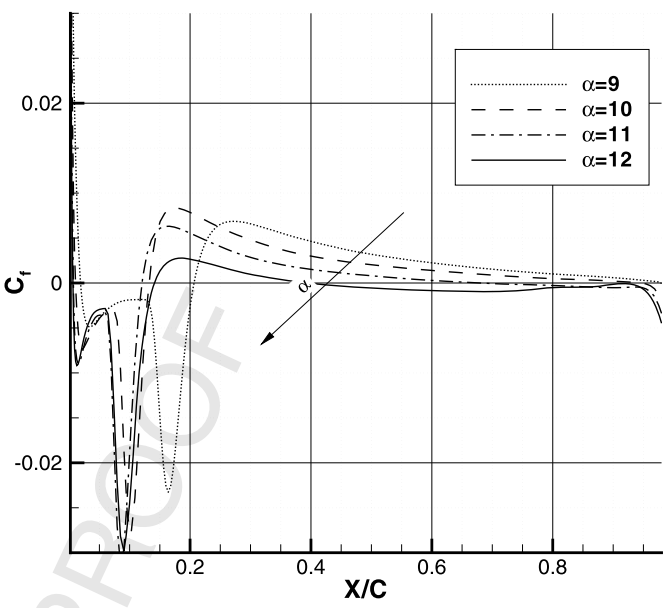


(b) Friction Coefficient

**Fig. 19.** SD7003 airfoil: evolution with $\alpha$ of the pressure and friction coefficient. $\kappa$–$\omega$ SST-LR turbulence model. ·····: $\alpha = 9°$, —: $\alpha = 10°$, -·-·-: $\alpha = 11°$, —: $\alpha = 12°$.

to HFWT, 2% with respect to Selig 96, 3% with respect to Selig 89 at $\alpha = 6°$). The $C_L$ provided by the $\kappa$–$\omega$ SST-LR model are very close to the ILES data and the difference with the experiments is always lower than 5%.

The implicit LES and the experiments from Selig show a stall at $\alpha = 11°$, while our large-eddy simulation yields a flow already stalled at this incidence. On the contrary, the $\kappa$–$\omega$ SST-LR model follows the ILES and experiments also at higher $\alpha$ and the stall prediction is in agreement with experiments and ILES.

### 3.3.2. Drag polar

The drag polar of the SD airfoil at Reynolds number $6.0 \times 10^4$ is presented in Fig. 16. The computed aerodynamic coefficients are compared to the measurements taken from Selig et al. in 1989 [21] and in 1996 [22].

Surprisingly, the numerical data, and in particular the results provided by the $\kappa$–$\omega$ SST-LR are in better agreement with the experiments performed in 1989 [21] than in 1996 [22], despite, according to Selig, 1996 results are considered more reliable because of the lower turbulence level in the wind tunnel. It is worth noting that a very large data scatter is present in the 1996 experiment and both LES and RANS results are in this scatter range, see Fig. 17. Indeed, data shown in Fig. 16 are averages of four measurements taken by wake inspection in four wing sections (Fig. 17). This result can be explained taking into account that the LSB phenomenon is highly unsteady and three-dimensional, making critical a comparison between an experiment and a *2D* numerical simulation.

### 3.4. Stall characteristics

Fig. 18 presents the streamlines and the eddy viscosity at several incidences achieved by the $\kappa$–$\omega$ SST-LR turbulence model. The turbulence begins to grow inside the bubble and then develops along the upper surface of the airfoil. The laminar separation bubble moves towards the leading edge as $\alpha$ increases. This displacement, noted also by other authors [9,29], is more pronounced at low-medium incidences up to $\alpha = 10°$. At higher incidences, as shown in Fig. 19, both the separation and re-attachment points do not vary considerably, but the recovery of the pressure decreases. A flow separation in the turbulence regime appears in the trailing edge zone at $\alpha = 11°$. The turbulent separation point moves upwards and the separated region becomes larger at $\alpha = 12°$. The flow at $\alpha = 12°$ re-attaches at a level of pressure significantly lower than at $\alpha = 11°$.

This analysis is confirmed by the unsteady visualization of the LES results at $\alpha = 12°$. Fig. 20 shows snapshots of the flow at four different times (scale is enlarged along the $y$ axis). Instantaneous span-wise velocity and streamlines are presented. The laminar separation bubble, shedding vortices and a turbulent separated zone in the backward part of the airfoil can be discerned. Vortices are shed from the laminar separated region in the forward part of the airfoil and flow into the next turbulent separated region. A large vortex is then convected from the airfoil. A similar shedding phenomenon is also shown in the large-eddy simulations performed by Yuan et al. [29].

## 4. Conclusions

A numerical analysis of the incompressible flow around the Selig–Donovan 7003 airfoil at Reynolds number $6.0 \times 10^4$ has been performed. RANS and large-eddy simulations are the methods applied. The RANS method is used for low-medium incidences. Time-accurate URANS simulations are performed at high angles of attack in order to achieve converged steady-state results.

The $\kappa$–$\omega$ SST-LR turbulence model has been employed in the RANS simulations.

The RANS methods require the knowledge of the point where the production of the turbulent kinetic energy is switched on in the turbulent transport equations. An empirical criterion, based on the analysis of published data and authors' large-eddy simulations, has been adopted to specify this point. The laminar separation bubble arising on the SD 7003 airfoil at Reynold number $6.0 \times 10^4$ is well captured and the results of the RANS simulations are in good agreement with the LES data.

The drag and lift curves of the airfoil have been computed, and the mechanism of the stall investigated. The $\kappa$–$\omega$ SST-LR model has provided a result comparable to the large-eddy simulation for either local and global aerodynamic coefficients. Both large-eddy simulations and URANS with the $\kappa$–$\omega$ SST-LR model have returned the same **type of** stall. The stall occurs when the laminar bubble



Please cite this article in press as: P. Catalano, R. Tognaccini, RANS analysis of the low-Reynolds number flow around the SD7003 airfoil, Aerospace Science and Technology (2011), doi:10.1016/j.ast.2010.12.006

$w$

Large-eddy simulation at

**Fig. 20.** 12°. Instantaneous span-wise velocity $v_\infty$.

Please cite this article in press as: P. Catalano, R. Tognaccini, RANS analysis of the low-Reynolds number flow around the SD7003 airfoil, Aerospace Science and Technology (2011), doi:10.1016/j.ast.2

present in the leading edge zone and a turbulent separated region, forming on the central part of the airfoil as the incidence increases, join together.

The main conclusion of the paper is that flows at low-Reynolds number and the peculiar phenomenon of the laminar separation bubbles can be simulated by the RANS approach. As the angle of attack increases and a converged solution is not easily recovered, time-accurate URANS simulations need to be performed. The choices of the turbulence model and of a proper transition location in the model itself resulted crucial. The $\kappa$–$\omega$ SST-LR model and an empirical criterion for the transition location have provided satisfactory results at least for the test-case presented in this paper.

## References

[1] R. Arina, C. Atkin, E. Hanff, K. Jones, T. Lekas, M. Oi, M. Khalid, B. McAuliffe, J.B. Paquet, M. Platzer, U. Rist, J. Windte, W. Yuan, Experimental and computational investigations in low Reynolds number aerodynamics with applications to micro air vehicles, RTO Technical Report NATO-AVT-101, NATO, 2009.
[2] P. Catalano, M. Amato, An evaluation of RANS turbulence modelling for aerodynamic applications, Aerospace Science and Technology Journal 7 (7) (2003) 493–509.
[3] P. Catalano, R. Tognaccini, Influence of free-stream turbulence on simulations of laminar separation bubbles, in: 47th AIAA Aerospace Sciences Meeting and Exhibit, Orlando, FL, AIAA paper 2009-1471, Jan. 3–Jan. 5 2009.
[4] P. Catalano, R. Tognaccini, Numerical analysis of the flow around the SD 7003 airfoil, in: 48th AIAA Aerospace Sciences Meeting and Exhibit, Orlando, FL, AIAA paper 2010-68, Jan. 4–Jan. 7, 2010.
[5] P. Catalano, R. Tognaccini, Turbulence modelling for low Reynolds number flows, AIAA Journal 48 (8) (2010) 1673–1685.
[6] P. Catalano, M. Wang, G. Iaccarino, P. Moin, Numerical simulation of the flow around a circular cylinder at high Reynolds numbers, International Journal of Heat and Fluid Flow 24 (2003) 463–469.
[7] M. Drela, M. Giles, Two-dimensional transonic aerodynamic design method, AIAA Journal 25 (9) (Sep. 1987) 1199–1206.
[8] J.H. Ferziger, M. Peric, Computational Methods for Fluid Dynamics, Springer-Verlag, Berlin & Heidelberg, 1996.
[9] M.C. Galbraith, M.R. Visbal, Implicit large eddy simulation of low Reynolds number flow past the SD 7003 airfoil, in: 46th AIAA Aerospace Sciences Meeting and Exhibit, Reno, NV, AIAA paper 2008-225, Jan. 7–Jan. 10, 2008.
[10] M. Germano, U. Piomelli, P. Moin, W.H. Cabot, A dynamic subgrid-scale eddy viscosity model, Physics of Fluids 3 (1991) 1760–1765.
[11] H.P. Horton, Laminar separation in two and three-dimensional incompressible flow, PhD thesis, University of London, 1968.
[12] W.P. Jones, B.E. Launder, The prediction of laminarization with a two-equation model for turbulence, International Journal of Heat and Mass Transfer 15 (1972) 301–314.
[13] J. Kim, P. Moin, Application of a fractional step method to incompressible Navier–Stokes equations, Journal of Computational Physics 59 (1985) 308–323.
[14] E. Lenormand, P. Saguat, L. Phuoc, P. Comte, Subgrid-scale models for large eddy simulation of compressible wall bounded flows, AIAA Journal 38 (2000) 1340–1350.
[15] D.K. Lilly, A proposed modification of the Germano subgrid scale closure method, Physics of Fluids 4 (1992) 633–635.
[16] C. Marongiu, P. Catalano, M. Amato, G. Iaccarino, U-zen: A computational tool solving U-RANS equations for industrial unsteady applications, in: 34th AIAA Fluid Dynamics Conference, Portland, OR, AIAA paper 2004-2345, Jun. 28–Jul. 1, 2004.
[17] F.R. Menter, Two-equation eddy viscosity turbulence models for engineering applications, Aerospace Science and Technology Journal 32 (7) (1994) 1598–1695.
[18] M.V. Ol, B.R. McAuliffe, E.S. Hanff, U. Scholz, C. Kalher, Comparison of laminar separation bubble measurements on a low Reynolds number airfoil in three facilities, in: 135th AIAA Fluid Dynamics Conference, Toronto, Canada, AIAA paper 2005-5149, Jun. 6–Jun. 9, 2005.
[19] R. Radespiel, J. Windte, U. Scholz, Numerical and experimental flow analysis of moving airfoils with laminar separation bubbles, in: 44th AIAA Aerospace Sciences Meeting and Exhibit, Reno, NV, AIAA paper 2006-0501, Jan. 3–Jan. 5, 2006.
[20] C.L. Rumsey, P.R. Spalart, Turbulence model behavior in low Reynolds number regions of aerodynamic flow fields, AIAA Journal 47 (4) (2009) 982–993.
[21] M.S. Selig, J.F. Donovan, D.B. Fraser, Airfoils at low speeds, in: Soartech 8, H.A. Stokely, Soartech Publications, Virginia Beach, VA, USA, 1989.
[22] M.S. Selig, J.J. Guglielmo, A.P. Groeren, P. Giguere, Summary of Low-Speed Airfoil Data, H.A. Stokely, Soartech Aero Publications, Virginia Beach, VA, USA, 1995.
[23] L. Tang, RANS simulation of low-Reynolds-number airfoil aerodynamics, in: 44th AIAA Aerospace Science Meeting and Exhibit, Reno, NV, AIAA paper 2006-0249, Jan. 3–Jan. 5, 2006.
[24] S. Wallin, A. Johansson, An explicit algebraic Reynolds stress model for incompressible and compressible turbulent flows, Journal of Fluid Mechanics 403 (2000) 89–132.
[25] M. Wang, P. Catalano, G. Iaccarino, Prediction of high Reynolds number flow over a circular cylinder using LES with wall models, in: CTR Annual Research Brief, 2001, pp. 45–50.
[26] D.C. Wilcox, Turbulence Modeling for CFD, DCW Industries Inc., La Canada, Los Angeles, California, 1994.
[27] J. Windte, U. Scholz, R. Radespiel, Validation of RANS simulation of laminar separation bubbles on airfoils, Aerospace Science and Technology Journal 10 (7) (2006) 484–494.
[28] W. Yuan, M. Khalid, J. Windte, U. Scholz, R. Radespiel, An investigation of low-Reynolds-number flows past airfoils, in: 23rd AIAA Applied Aerodynamics Conference, Toronto, Canada, AIAA paper 2005-4607, Jun. 6–Jun. 9, 2005.
[29] W. Yuan, H. Xu, M. Khalid, R. Radespiel, A parametric study of LES on laminar-turbulent transitional flows past an airfoil, International Journal of Computational Fluid Dynamics 20 (1) (Jan. 2006) 45–54.



Please cite this article in press as: P. Catalano, R. Tognaccini, RANS analysis of the low-Reynolds number flow around the SD7003 airfoil, Aerospace Science and Technology (2011), doi:10.1016/j.ast.2010.12.006